International Journal of Adhesion & Adhesives 68 (2016) 369–378

Contents lists available at ScienceDirect

International Journal of Adhesion & Adhesives

journal homepage: www.elsevier.com/locate/ijadhadh

Cohesive/adhesive failure interaction in ductile adhesive joints Part II: Quasi-static and fatigue analysis of double lap-joint specimens subjected to through-thickness compressive loading

Jonathan P.-H. Belnoue [a,*], Stefanos Giannis [b], Matthew Dawson [c], Stephen R. Hallett [a]

[a] Advanced Composite Centre for Innovation and Science (ACCIS), University of Bristol, Queen's Building, University Walk, Bristol, BS8 1TR, UK
[b] Element Materials Technology, Wilbury Way, Hitchin, SG4 0TW, UK
[c] Aviation Enterprises Ltd., Membury Airfield, Lambourn, RG17 7TJ, UK

ARTICLE INFO

Article history:
Accepted 4 November 2015
Available online 19 March 2016

Keywords:
Ductile adhesive
Cohesive zone modelling
Adhesive failure
Cohesive failure
Fatigue life prediction

ABSTRACT

This paper proposes a new methodology for the finite element (FE) modelling of failure in adhesively bonded joints. Cohesive and adhesive failure are treated separately which allows accurate failure predictions for adhesive joints of different thicknesses using a single set of material parameters. In a companion paper (part I), a new smeared-crack model for adhesive joint cohesive failure was proposed and validated. The present contribution gives an in depth investigation into the interaction among plasticity, cohesive failure and adhesive failure, with application to structural joints. Quasi-static FE analyses of double lap-joint specimens with different thicknesses and under different levels of hydrostatic pressure were performed and compared to experimental results. In all the cases studied, the numerical analysis correctly predicts the driving mechanisms and the specimens' final failure. Accurate fatigue life predictions are made with the addition of a Paris based damage law to the interface elements used to model the adhesive failure.

1. Introduction

Recent progresses in adhesive joint technology (e.g., tougher systems and better surface preparation) [1,2] have resulted in an increased use of adhesive bonds in the design of engineering components of increased complexity, subjected to increasingly challenging mechanical loading and environment. For example, adhesive joints have now been integrated in the design of rotating engines such as tidal and wind turbines where the ability of the structural components to resist fatigue failure is of prime importance. Traditionally adhesive joints have been designed in such a way that failure cannot happen in the joint [1]. Whilst being the safest option, this results in levels overdesign and the resulting costs that are not sustainable for the industry.

In recent years, methods aiming at improving the reliability of numerical tools for fatigue failure predictions of adhesive bond have been proposed [3–10]. Like their quasi-static failure equivalent [11], these models are primarily based on the cohesive zone method (CZM). Most of these models however do not take account of the adhesive plastic deformation. This is potentially an impediment for accurate fatigue life prediction in adhesive joints involving new tougher (i.e., more ductile) systems. Fatigue failures mostly occur whilst the adhesive is in the elastic regime. Adhesive plastic deformation can however be responsible for up to 80% of the joint strength [12] and consequently has a non-negligible influence on the severity of the applied fatigue cycles.

In the "science of adhesive joints," adhesive failure is generally not accepted as it is often the result of poorly made and/or designed joints. Therefore, most adhesive joints models available in the literature tend to disregard it or, at best, lump all the fracture mechanisms together. This often gives rise to phenomenological models using material parameters whose physical nature is not always easy to understand and showing a fairly narrow range of applicability. Even though this approach works well for industry purposes, it is harder to justify from an academic point of view as it does not give much room for deeper understanding of the physical phenomena leading to the joints' failure. In the case of quasi-static failure, Pardoen and Kinloch [13–15] have performed in depth experimental and numerical analysis of the influence exerted by the joint plasticity on its overall strength. The present contribution explores in more detail the competition between adhesive and cohesive failure of ductile adhesives. Particular emphasis is placed on an industrially relevant steel to composite

* Corresponding author. Tel.: +44 117 33 15798.
E-mail address: jonathan.belnoue@bristol.ac.uk (J.-H. Belnoue).

http://dx.doi.org/10.1016/j.ijadhadh.2016.03.010

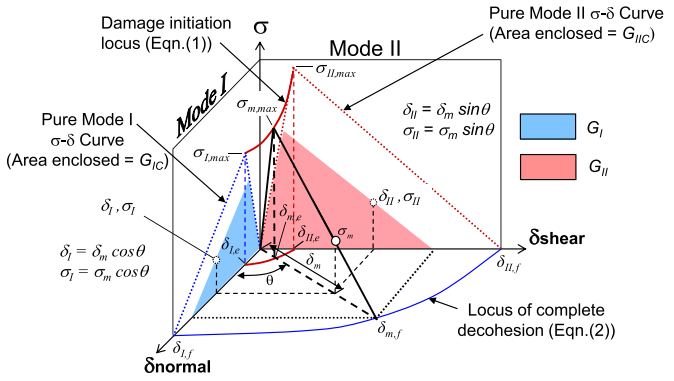

Fig. 1. The mixed-mode traction separation response [17].

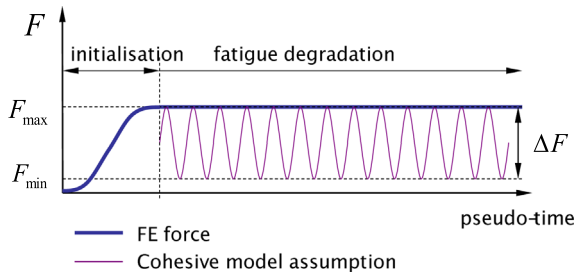

Fig. 2. Modelling the envelopes of loads and displacements in a cyclic regime.

double lap-joint specimen that fails under different modes for different levels of hydrostatic pressure and depending on whether loaded statically or cyclically. The modelling of the joint represents the adhesive with the smeared-crack model for cohesive failure presented in part I [11]. Adhesive failure is modelled through the insertion at the adhesive/composite interface of a layer of cohesive elements. Numerical analysis clearly suggests that both failure mechanisms need to be considered to predict accurately the specimen strength.

2. Adhesive failure modelling

2.1. Static loading

Interfacial failure that may arise from debonding of the adhesive was modelled using cohesive elements with a bi-linear traction–separation law [16]. Under mixed mode loading, the formulation can be illustrated using a single three-dimensional map by representing the normal opening mode (mode I) on the 0–σ–δ_{normal} plane, and the transverse shear mode (mode II) on the 0–σ–δ_{shear} plane, as shown in Fig. 1. The triangles 0–$\sigma_{I,max}$–$\delta_{I,f}$ and 0–$\sigma_{II,max}$–$\delta_{II,f}$ are the responses in pure opening mode and in pure shear mode respectively. Any point on the 0–δ_{normal} –δ_{shear} plane represents a mixed-mode relative displacement.

The mixed mode damage onset displacement, $\delta_{m,e}$, and interfacial strength, $\sigma_{m,max}$, are calculated using a quadratic damage onset criterion:

$$\left(\frac{\max(\sigma_I, 0)}{\sigma_{I,max}}\right)^2 + \left(\frac{\sigma_{II}}{\sigma_{II,max}}\right)^2 = 1 \tag{1}$$

The failure displacement corresponding to complete decohesion, $\delta_{m,f}$, is calculated from the following failure criterion:

$$\frac{G_I}{G_{IC}} + \frac{G_{II}}{G_{IIC}} = 1 \tag{2}$$

where G_{IC} and G_{IIC} are the critical energy release rates for pure mode I (opening) and pure mode II (shear), respectively.

The accumulation of irreversible damage can then be tracked using the static damage parameter, d_S, defined as follows (Fig. 2):

$$d_S(\delta_m) = \frac{\delta_m - \delta_{m,e}}{\delta_{m,f} - \delta_{m,e}} \tag{3}$$

The element complete failure occurs when d_S reaches a value of unity.

A modification of the interface element formulation which takes into account the enhancement in effective mode-II properties when the interface is under through-thickness compressive stresses is used here. It is assumed that the initial cohesive stiffness and softening slope remain constant, and the effective mode-II strength is then given by

$$\sigma'^{max}_{II} = \sigma^{max}_{II} - \eta\sigma_{33} \tag{4}$$

where σ_{33} is the through-thickness stress, σ^{max}_{II} is the mode-II strength in the absence of through-thickness stresses, and η is an empirically derived enhancement factor analogous to an internal friction coefficient. The effective critical mode-II strain energy release rate becomes

$$G'_{IIC} = \left(\frac{\sigma'^{max}_{II}}{\sigma^{max}_{II}}\right) G_{IIC} \tag{5}$$

A value of $\eta = 0.3$ was set. This value should ideally be measured experimentally for the specific material in use. However, this was not available and so the value used was chosen consistent with the value measured by Gan et al. [18] in the case of an epoxy-matrix composite. Cognard et al. [19] have measured the elastic limit of an epoxy adhesive in a bonded assembly under different levels of hydrostatic pressure. Fitting their data with a very simple Mohr–Coulomb criterion also leads to a value for η very close to 0.3, thus further justifying the choice of this value.

2.2. Fatigue loading

In the last few years, algorithms to include fatigue damage accumulation in the cohesive element formulation have been developed [17,20–23]. These incorporate the Paris law for crack growth, where the crack growth rate, $\frac{\partial a}{\partial N}$, is characterized with respect to the change in crack tip strain energy release rate, ΔG, within each fatigue cycle using the following relationship:

$$\frac{\partial a}{\partial N} = C\left(\frac{\Delta G}{G_C}\right)^m \tag{6}$$

The parameters C and m are constants derived by curve fitting experimental data.

For the more common case of mixed mode loading, the Paris law constants, C and m, are calculated from the, experimentally measured, pure mode I and pure mode II coefficients using a simple linear rule of mixtures between modes I and II as proposed by Russell and Street [24]:

$$C_m = C_I\left(\frac{G_I}{G_T}\right) + C_{II}\left(\frac{G_{II}}{G_T}\right)(a) m_m = m_I\left(\frac{G_I}{G_T}\right) + m_{II}\left(\frac{G_{II}}{G_T}\right)(b) \tag{7}$$

In these equations, the subscripts m, I and II are used to distinguish between the experimentally derived mode I and mode II Paris law constants and the calculated mixed mode Paris law constants. G_T is the total strain energy release rate: $G_T = G_I + G_{II}$. More sophisticated rules such as the one described by Blanco et al. [25] could be used and may give greater accuracy. However, these rules would necessitate the experimental determination of a third (mixed-mode) point that was not available for the material system used in the present work.

In the numerical fatigue model, it would be too computationally expensive to model each fatigue cycle explicitly. An envelope

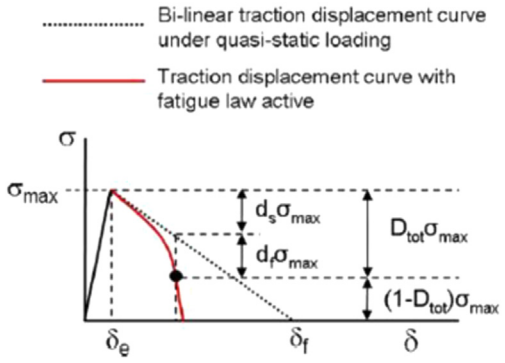

Fig. 3. Static and fatigue damage parameters in relation to the interface element traction-separation curve [17].

of the maximum cyclic load is thus applied instead. When the fatigue law becomes active, interface elements acquire damage under the assumption that the load varies between the maximum and the minimum load within each fatigue cycle, as shown in Fig. 3.

The use of the envelope loading means that the change in strain energy release rate within each fatigue cycle, ΔG, required by the Paris law must be calculated using the following expression:

$$\Delta G = G_{max}\left(1-R^2\right) \tag{8}$$

where R is the load ratio, which is supplied as a user input within the model and G_{max} is the maximum strain energy release rate within each fatigue cycle which is extracted from the model by integrating each interface element's traction–separation response. A cycle frequency is also required by the model, supplied as a user input, to define the number of fatigue cycles per unit of analysis time (pseudo-time).

The introduction of an additional fatigue damage parameter, d_f, so that the total damage accumulated, D_{tot}, becomes

$$D_{tot} = d_S + d_f \tag{9}$$

allows taking into account the accumulation of damage during fatigue loading (see Fig. 1).

The crack tip tracking algorithm proposed by Kawashita and Hallett [20] (which is a refinement of the Harper and Hallett [17] fatigue modelling technique) is used. The main advantage of this method is the independence of results from the cohesive zone length in the model (which is a geometry and material dependent parameter) and its relative insensitivity to mesh refinement. This is achieved by considering that only the elements situated at the crack front can accumulate fatigue damage whilst the other elements in the cohesive zone can continue to accumulate only static damage. Fatigue damage accumulation in the elements at the crack tip will influence the formation of the entire cohesive zone through stress redistribution, but the energy balance, as determined by the Paris law, will remain correct, without further calibration factors. The crack will then propagate as the crack tip elements reach complete failure by the formation of a new crack tip (in which the elements can accumulate fatigue damage) Readers are referred to Ref. [20] for full details, where this model was applied and validated for the case of delamination in epoxy-matrix composites. Calling L_{el} the interface element length in the direction of the crack propagation, the crack advances the distance L_{el} after a number of cycles, ΔN_e, has elapsed. At every time step, t, the additional damage required to cause point-wise failure of the integration point under consideration is $\Delta D = 1 - d_S$ (see Fig. 1).

The fatigue damage rate can be calculated from

$$\frac{\partial d_f}{\partial N} = \frac{\Delta D}{\Delta N_e} = \frac{1-d_S}{L_{el}}\frac{\partial a}{\partial N} \tag{10}$$

where $\frac{\partial a}{\partial N}$ is determined using Eqs. (6) and (7) and the experimentally measured values for C_I, C_{II}, m_I and m_{II} supplied as a user input. Using Eq. (9), it is possible to update the damage parameter at time t. Eq. (9) is finally used to compute the total damage accumulated at the interface which allows in return to compute the stress carrying capacity of the point under scrutiny.

3. FE model

3.1. Test case

The validation of the proposed method and its relevance as a design tool for adhesive joints is demonstrated here, comparing the model predictions with experimental data collected from quasi-static and fatigue testing of a steel to composites double lap-joint specimen subjected to in-plane tension loading, with additional through-thickness compressive stress. The test geometry (see Fig. 4) was carefully selected to ensure failure of the bond before either of the substrates. It is a sufficiently simple design for ease of testing, but also sufficiently complex to provide a good test case for the numerical models and to be representative of engineering features used in industry. Hence, the through-thickness compression applied on the specimen's surfaces simulates bolting pressure (which is often found in the design of engineering components) and provides a very good test case of the model abilities to take account of the influence of the hydrostatic pressure on the joint failure. It was chosen to use the same commercial adhesive as in part I [11]. Crack initiation was facilitated through the insertion of a 5 mm-wide band of PTFE allowing the creation of a pre-crack at the interface between the adhesive and the composites adherend. This way the industrial "worst case" of a bondline that is not fully formed or a small piece of composite release film left in the joint during manufacture was simulated.

The specimens were tested under static and cyclic tensile loading (with a load ratio $R = 0.1$), with the test setup shown in Fig. 5a. For quasi-static tests, the specimen strengths were recorded. Under fatigue loading, different severities were considered, thus allowing the extraction of the S–N curves. Specimens with 1 mm and 2 mm thick bondlines were tested. Through-thickness compression was applied and could be varied through an arrangement of 4 screws connected to a load cell. All series of tests were first performed with no pressure applied on the specimens surfaces and then repeated with through-thickness compression of 5 MPa, 10 MPa and 15 MPa, respectively. As illustrated in Fig. 5b, the specimens clearly failed from the combined effect of cohesive (i.e., rupture of the adhesive bulk material) and adhesive failure (i.e., interfacial failure or debonding of the adhesive). One of the key aims of the present work is to predict the interaction between the two failure mechanisms and to show how the proposed modelling approach can help in this task.

3.2. Modelling strategy

Static and fatigue analyses have been conducted on FE models (see Fig. 4b) for all the tested specimens, enabling a comparison between numerical and experimental results. All of the adhesive and interface element formulations detailed in Section 1 of the present paper and in the companion (part I) paper [11] were developed within the explicit finite element code LS-Dyna.

As illustrated in Fig. 4b, in the FE model, the steel end of the specimen was fixed, whilst the composite end was loaded in

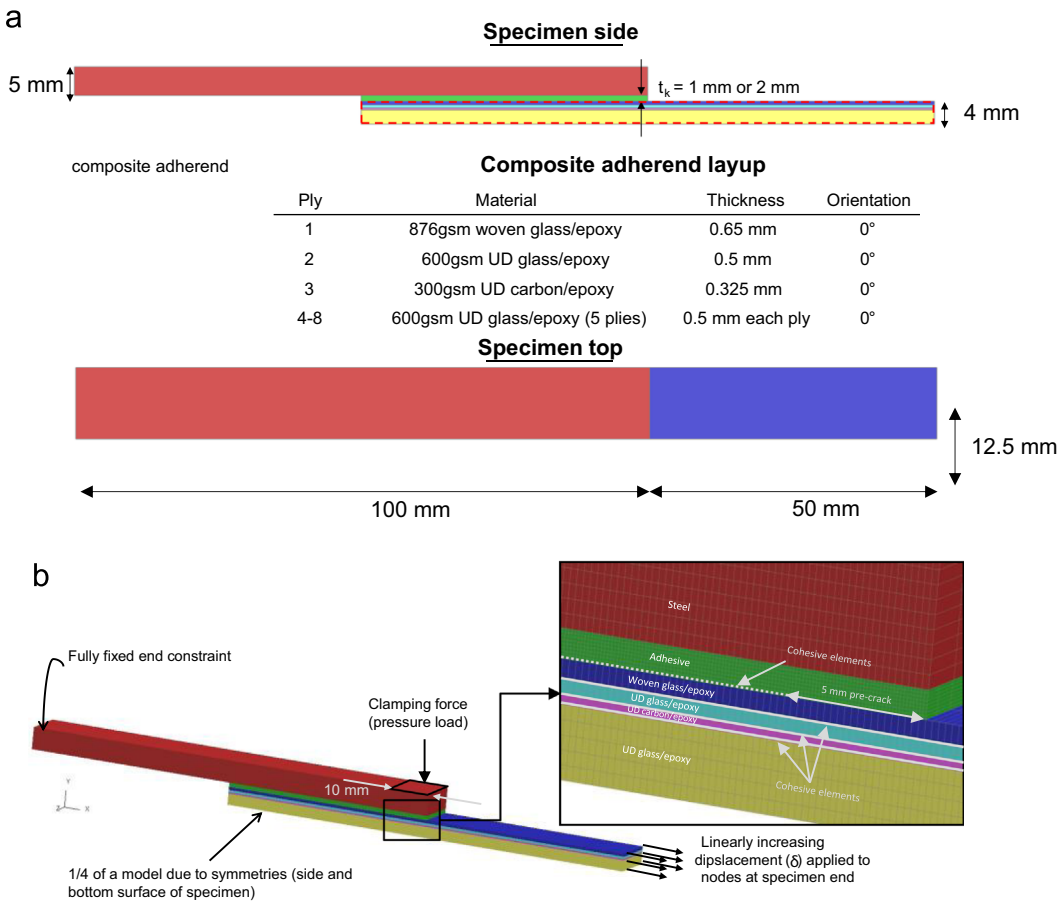

Ply	Material	Thickness	Orientation
1	876gsm woven glass/epoxy	0.65 mm	0°
2	600gsm UD glass/epoxy	0.5 mm	0°
3	300gsm UD carbon/epoxy	0.325 mm	0°
4-8	600gsm UD glass/epoxy (5 plies)	0.5 mm each ply	0°

Fig. 4. Double lap-joint specimen geometry (a/) and model setup (b/).

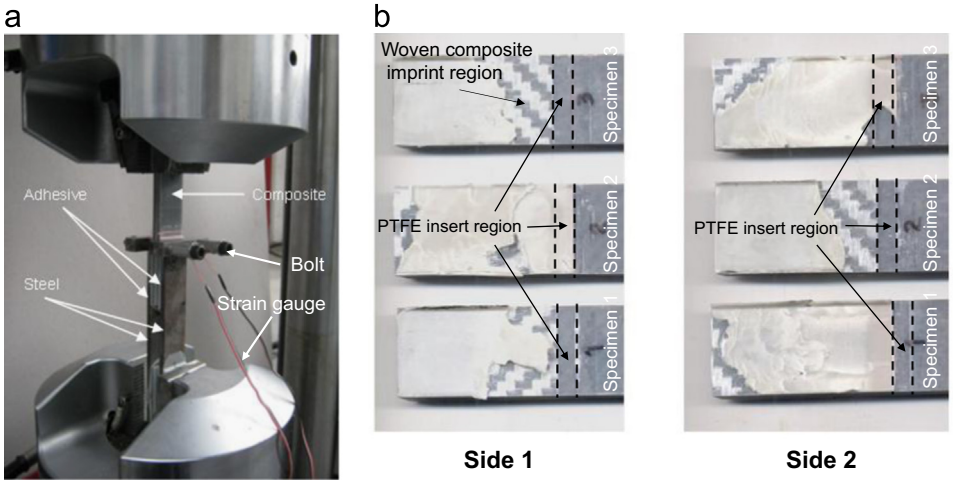

Fig. 5. (a) Experimental setup. (b) Composite adherends' surfaces after complete failure of the specimens indicating the presence of 2 competing failure mechanisms. Failure can occur at the adhesive/composite interface (see Side 2 of Specimen 2), in the adhesive bulk material or be a mix of both failure modes (this is the case in most of the specimens here). Images are from 1 mm thick joint statically loaded with no through-thickness pressure.

tension. The quasi-static analyses were run under displacement control. Fatigue analyses on the other hand were run under load control. Due to the specimen symmetry, a quarter model was used, with nodes along the through-thickness plane of symmetry restrained from out of plane translation and on the transverse symmetry plane restrained from horizontal motion. The specimen constituents were modelled using 8 noded single integration point solid elements. Fig. 6 shows information on the element sizes used. The meshing strategy adopted was to find the right balance between model accuracy and CPU cost. Mass was scaled by a factor of 10^5, which resulted in relatively short computational times (less than 2 days) while still avoiding significant dynamic effects for quasi-static and fatigue loading scenarios. Hence, only 1 element per ply was used in the composite thickness direction. Moreover, LS-Dyna's TIED_CONTACT option permitted the use of a relatively refined mesh in the adhesive and a coarser mesh in the other specimen constituents. Finally, in the transverse direction of the adhesive, a biased mesh allowed the use of smaller elements at the

specimen edges than at the specimen centre. This allowed capturing of the stress and strain distribution at the crack tip adequately. A similar procedure was employed for the cohesive element layer placed to simulate interfacial failure at the adhesive/composite interface.

The steel adherend was represented as an isotropic perfectly elastic solid (with Young's modulus and Poisson ratio set to 207 GPa and 0.3, respectively) and the composite plies were modelled using anisotropic perfectly elastic materials (with the material properties given in Table 1). Potential delaminations within the composite material were taken into account by inserting a layer of cohesive elements between each of the constituents of the composite adherend (see material properties in Table 2). Interfacial properties were measured following the procedure described in [26]. In order to ensure conservative model predictions, interfacial properties were set equal to those of the weaker of the two constituent systems of each interface.

The necessity to take account of both cohesive and adhesive failure for accurate strength predictions is highlighted comparing the results obtained from 3 different modelling strategies of the bonded joint with the experimental results:

- In the first scenario tested, only adhesive failure was considered. The adhesive bulk material was modelled as a perfectly plastic material (experimental measurements in the part I paper [11] suggest that this is a sufficiently accurate approximation) and a layer of cohesive element accounting for the adhesive debonding was introduced at the adhesive/composite interface.
- In the second case, the specimen could only fail through cohesive failure. The adhesive was modelled with a new material model for cohesive failure presented in part I [11] that uses a smeared-crack approach, where the adhesive plasticity is represented through a (pressure dependent) Drucker–Prager criterion. The layer of cohesive element introduced at the composite adhesive interface (i.e., the dotted line in Fig. 7b) was removed.
- Finally, in the last case, both adhesive and cohesive failure were considered.

In the last two cases, the material properties used for the commercial adhesive were the same as those used in the part I paper [11] and are reported in Table 2. When considered, the interfacial properties for adhesive failure were set to the values given in Table 3. These experimental data were derived from ELS and DCB tests on samples of adhesively bonded steel plates, following the same procedure as described in [26]. The interfacial strengths were slightly modified so that the stresses in the interface never exceed those of the adhesive [27]. Fatigue capabilities were subsequently activated in the cohesive interface elements for adhesive failure only.

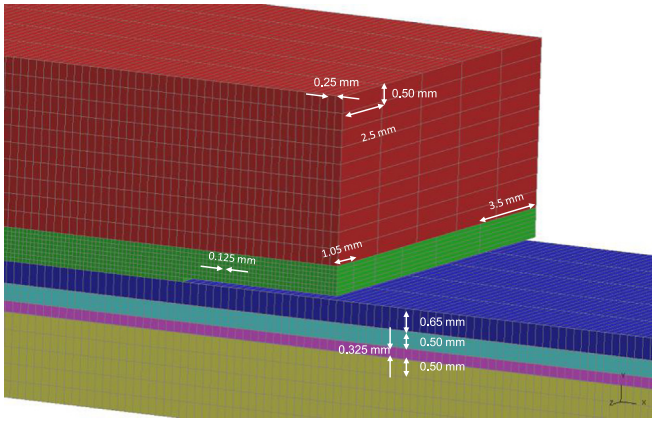

Fig. 6. Element size used for the double lap-joint test mode.

4. Results and validation

4.1. Static loading

Fig. 7a and b shows the importance of taking account of both adhesive and cohesive failure. When only adhesive failure was considered (i.e., light grey dotted lines in Fig. 7), the experimental data were well matched for low values of the through thickness compression; on the other hand, cohesive failure models (i.e., dark grey dotted line in Fig. 7) performed best for high values of the clamping force. Introducing both failure mechanisms in the model allowed matching the experimental data well. It is important to note that the model predictions where the two failure mechanisms were considered never quite matched those obtained when only cohesive or adhesive failure was considered. This demonstrates the model's ability to capture the interactions between adhesive and cohesive failure that was observed in the experiment (see Fig. 5b). This is confirmed by the study of predicted damage

Table 1
Material properties (as given by the manufacturer) applied in numerical models to the 3 composite systems.

	Woven glass/epoxy	UD glass/epoxy	UD carbon/epoxy
E_{11} (GPa)	27.64	38.7	118
E_{22} (GPa)	28.23	11.83	7.24
E_{33} (GPa)	11.83	11.83	7.24
G_{12} (GPa)	4.03	3.85	3.96
G_{13} (GPa)	3.02	3.85	3.96
G_{23} (GPa)	3.02	1.93	1.98
ν_{12}	0.18	0.29	0.33
ν_{13}	0.35	0.29	0.33
ν_{23}	0.35	0.40	0.4

Table 2
Material properties applied in numerical models to the adhesive. $E_{adhesive}$ is Young's modulus, $\upsilon_{adhesive}$ is the Poisson ratio and the energy necessary to cleave the bulk material under shear loading is called G_C^{shear}.

$E_{adhesive}$ (GPa)	$\upsilon_{adhesive}$	G_C^{shear} (N/mm)
2.3	0.3	4.15

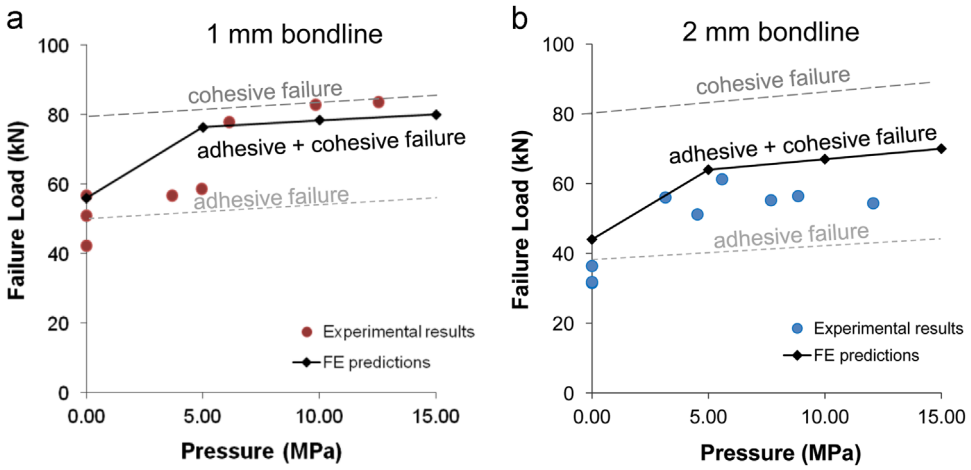

Fig. 7. Effect of the clamping force on the specimen for the 1 mm-thick joint specimen, experimental results and numerical predictions.

Table 3
Interfacial properties used in the numerical models.

	Woven glass/epoxy – UD glass/epoxy interface	UD glass/epoxy – UD carbon/epoxy interface	Adhesive/composite adherend interface
G_{Ic} (N/mm)	0.302	0.212	0.4
G_{IIc} (N/mm)	1.381	1.155	0.8
$\sigma_{I,max}$ (MPa)	22.68	13.26	32.0
$\sigma_{II,max}$ (MPa)	61.87	71.0	48.5
k_I (N/mm^3)	1.0E5	1.0E5	1.0E5
k_{II} (N/mm^3)	1.0E5	1.0E5	1.0E5
C_I			0.0991
C_{II}			0.4672
m_I			3.18
m_{II}			3.16

development at the adhesive/composite interface and in the adhesive presented in the next section.

4.1.1. *Influence of the through thickness compression*

Figs. 8 and 9 illustrate the damage evolution in the later stages of the deformation process in the 1 mm-thick joint specimen when no pressure and a 5 MPa pressure load is applied on the specimen surfaces. In both cases, final failure occurred from adhesive debonding. When no pressure was applied on the specimen surfaces, cohesive damage appeared only at a very late stage of the deformation process when catastrophic interfacial failure was already well on its way. In contrast, with a 5 MPa pressure applied on the specimen surfaces, significant cohesive damage was observed well before the interfacial crack started to propagate catastrophically. Under the influence of the through-thickness compressive stresses, most of the deformation occurs in the adhesive and the crack propagates at the interface only because it is significantly weaker than the adhesive. It is however interesting to note that when only adhesive failure is considered (despite taking account of the adhesive plasticity), the increase of the specimen strength with the clamping force magnitude is not as pronounced as when both failure criteria are active. This seems to confirm that the observed behaviour is a direct consequence of the interaction of cohesive and adhesive damage. It can thus be postulated that damage-induced softening in the adhesive slows down damage propagation at the interface by making it harder to satisfy the damage initiation condition of Eq. (1); as a result, elastic unloading of the adhesive is slowed down and more plastic energy can be dissipated through plastic straining of the adhesive, thus resulting in increasing specimen's strength. Overall, more cohesive rupture is observed in the experimental data (see Fig. 5b) than predicted by the models.

It is important to note that the models assume the adhesive to be homogeneous. In reality, inhomogeneities in the joint (such as air bubble entrapment, poor mixing, contaminants, etc.) are unavoidable. It is therefore more than likely that the cohesive damage observed in the numerical models would develop further as a fully developed crack should the inhomogeneities be taken into account.

4.1.2. *Joint thickness influence*

Comparing Fig. 7a and b shows a strong influence of the thicknesses on the specimen strengths. Moreover, when only cohesive failure is considered, the predicted strengths do not seem to vary with the thickness. This suggests that the observed difference is not due to constraint effect. Fig. 10, in which the spatial distribution of the total strain energy release rate dissipated through adhesive failure is plotted for the 1 mm- and 2 mm-thick samples (with no pressure applied on the specimens' surfaces), provides a good explanation of the phenomenon. The larger mode I component in the 2 mm-thick samples and associated lower fracture toughness results in a weaker interface than for the 1 mm-thick sample that has a high mode II component. A stronger interface not only requires more energy to cause failure but also allows the adhesive to deform further and dissipate additional energy through plastic straining. This results in higher specimen strength.

4.2. *Fatigue loading*

Finally, a prediction of fatigue life from the numerical models was performed. Despite the somewhat simplified modelling strategy adopted here (i.e., the fatigue capabilities were only implemented in the layer of cohesive elements simulating the

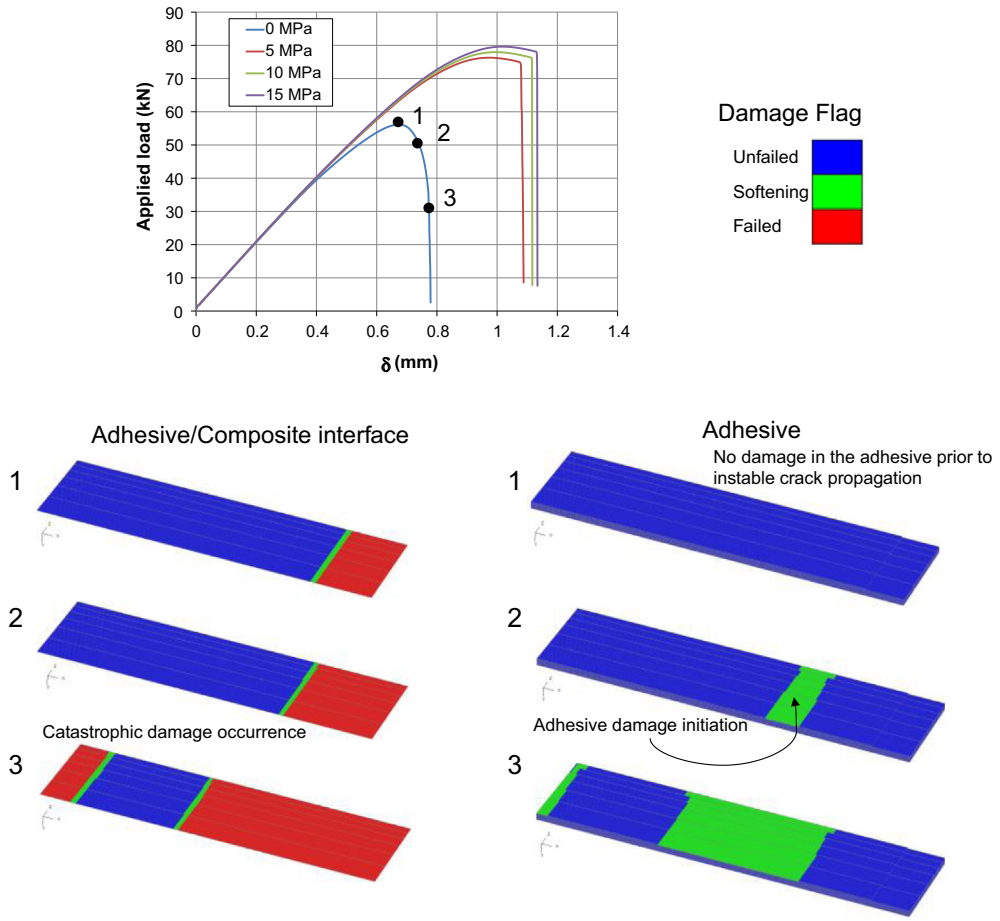

Fig. 8. Damage evolution in the adhesive and the adhesive/composite interface when the 1 mm-thick joint double lap-joint specimen is loaded statically and no pressure is applied on the specimen side.

debonding of the adhesive, the material parameters used correspond to a steel/adhesive interface, etc.), very good results are obtained. Fig. 11 illustrates the comparison between numerically predicted and experimentally measured S–N curves for samples of different thicknesses and different levels of through thickness compression, normalised by the static result. A normalised plot is a better indication of the performance of only the fatigue predictions, and any inaccuracies are not carried over from the static performance of the model, which has been evaluated in the previous section. The good quality of the results obtained can be attributed to the fact that, no matter the joint thicknesses or the magnitude of the through-thickness compression, all specimens ultimately fail through adhesive failure. Introducing fatigue capabilities for adhesive debonding only is therefore a reasonable approximation in this case. It is worthwhile to note that despite the same Paris curve being given as an input to all of the simulations, the models are able to capture the experimentally observed improvement of the fatigue life with an increased through-thickness compressive load. This is a direct consequence of Eq. (10) where the evolution of the fatigue damage is dependent on the level of static damage accumulated at the interface. As observed in Section 4.1.1, when a clamping force is applied on the specimens' sides, extensive cohesive damage develops in the adhesive prior to the apparition of adhesive damage (which is the driving mechanism for final failure); the resulting softening in the adhesive makes it harder for the static damage at the interface to develop and slows down the accumulation of fatigue damage.

5. Conclusions

In a recent review paper dedicated to fatigue prediction of bonded joints, Pascoe et al. [28] highlighted the necessity to fight against the temptation of continuously enriching the state of the art modelling techniques with an increasing number of parameters of rather doubtful physical meaning every time modelling predictions do not quite match the observed macroscopic behaviour of the material. They recommended to instead trying "to concentrate on elucidating the link between the physical processes involved (…) and the resultant macroscopic behaviour." The same recommendation could also be applied to the modelling of adhesive joints when loaded statically. The present contribution has aimed to make a step in this direction.

Traditional modelling techniques of adhesive joints tend to lump all the cracking phenomenon involved (i.e., plasticity, adhesive failure and cohesive failure) into one single cohesive law. This allows accurate prediction for specimen strength when appropriately calibrated. However, the method does not give much information about other key design parameters such as the risk of adhesive failure which is prohibited in adhesive joint design. The present paper proposes a new method for adhesive joint failure prediction whereby adhesive and cohesive failures are treated separately. Adhesive failure is modelled by introducing a layer of bi-linear cohesive elements at the interface between the adhesive and the adherend, cohesive failure is simulated through the use of a new smeared crack model introduced in a companion (part I) paper [11]. As the adhesive plastic deformation, cohesive and

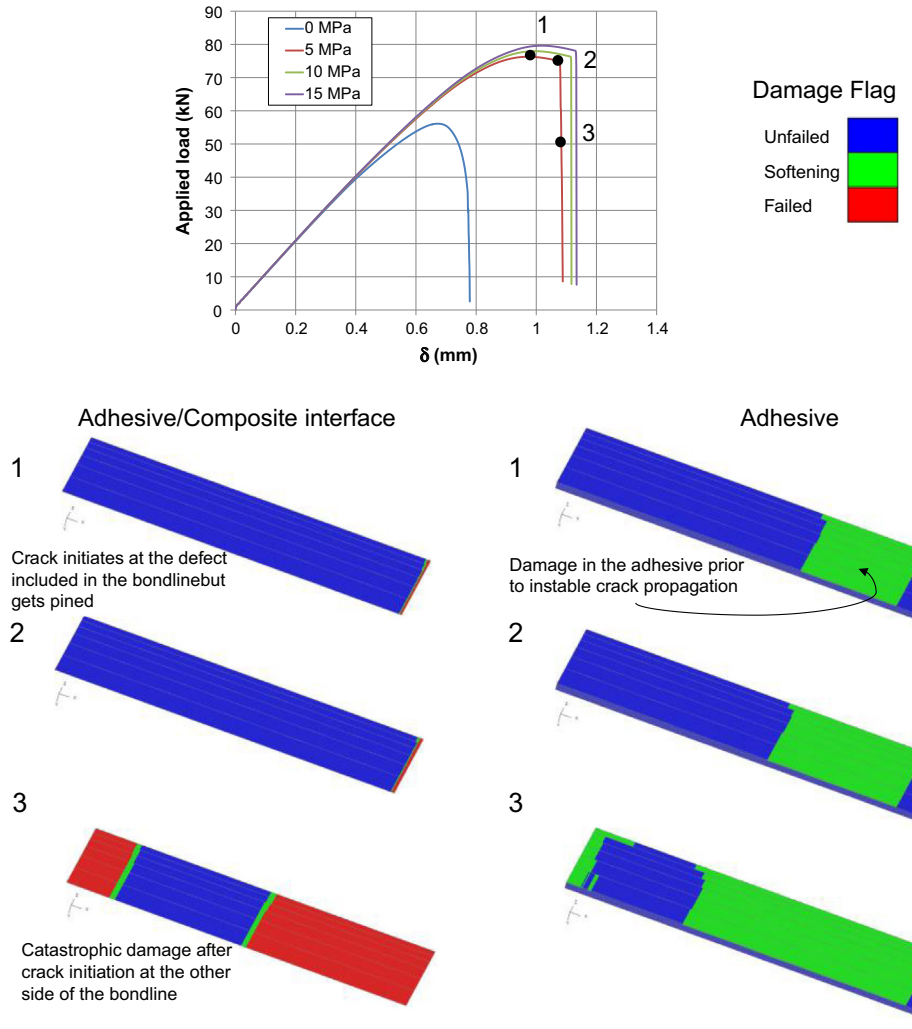

Fig. 9. Damage evolution at the adhesive/composite interface and in the adhesive when the 1 mm-thick joint double lap-joint specimen is loaded statically and a 5 MPa pressure is applied on the specimen side.

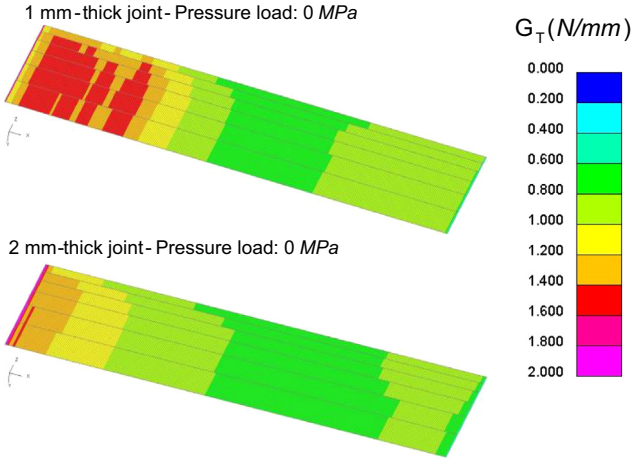

Fig. 10. Spatial distribution of the total strain energy release rate dissipated by the cohesive elements situated at the adhesive/composite interface for the 1 mm- and 2 mm-thick joints. No clamping force was applied on the specimen sides.

adhesive damage are all explicitly represented within the model, no calibration of the material parameters is necessary to take account of these phenomena and their interactions. Using the proposed methodology, it was possible to accurately predict strength and fatigue life of steel to composite double lap joint specimens of different thicknesses subjected to different levels of through-thickness compression using a single set of material parameters. In every case, the model was able to predict the failure mode (i.e., cohesive failure, adhesive failure or a mix of both) under which the specimen ultimately failed. This provided a very good validation of the proposed methodology and also (indirectly) of the newly proposed smeared crack model for cohesive failure.

The main drawback of the proposed method is that it is relatively heavy in terms of material characterisation. The adhesive

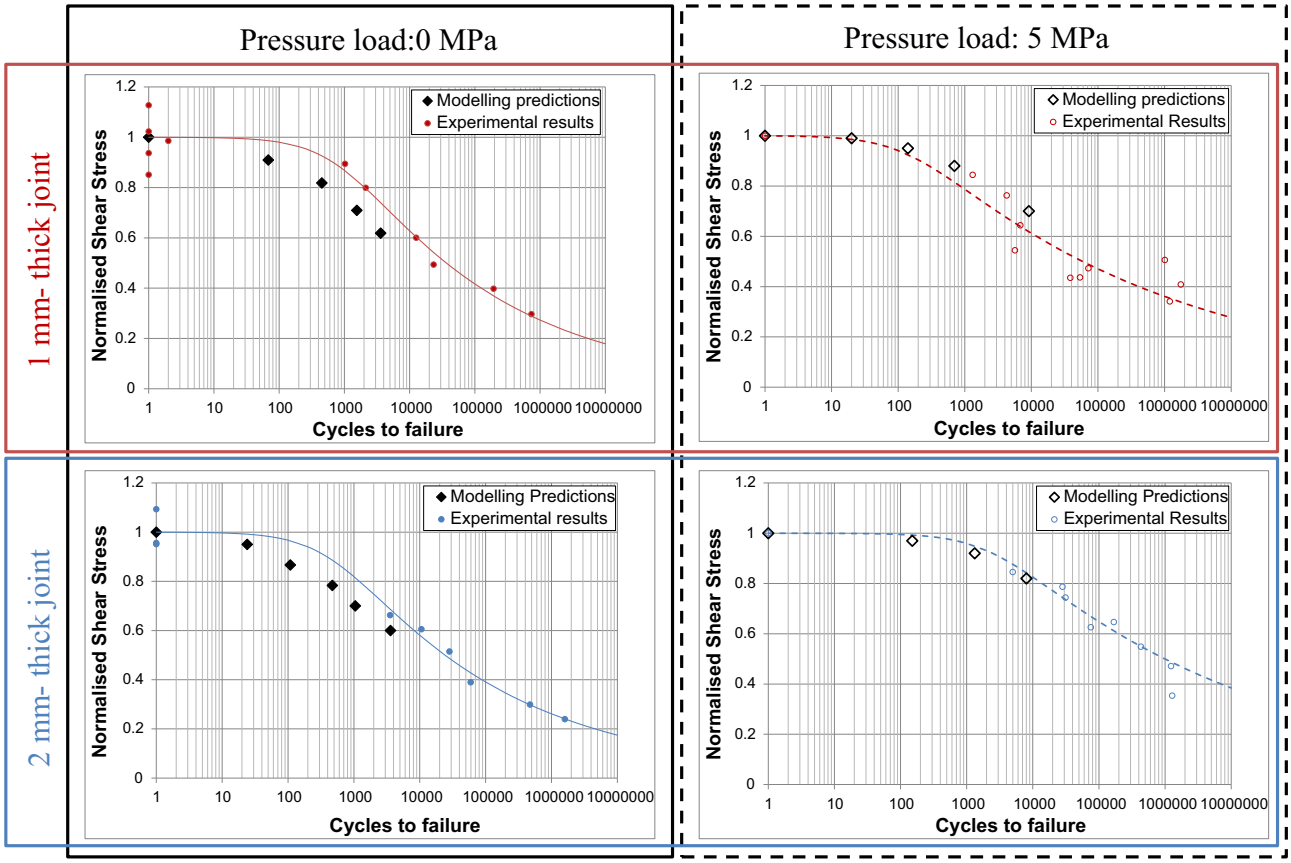

Fig. 11. Experimental and numerical normalised S–N curves for the 1 mm (top) and 2 mm-thick (bottom) joint specimens with (right) and without (left) 5 MPa pressure load applied on the surfaces.

bulk material is described through its hardening curves under 2 distinct loading modes (e.g., pure tension and pure shear) and the energy necessary to cleave it under shear loading. Adhesive failure is modelled through a simple bi-linear cohesive law with its behaviour under static loading being determined by 4 parameters: the mode I and mode II interfacial strengths and the mode I and mode II fracture energies. If fatigue loading is considered, mode I and mode II crack growth curves are also required.

The paper highlights the significant importance of being able to accurately model the failure process under quasi-static loading to then be able to perform accurate fatigue life predictions. More generally, it shows that providing that the underlying physical mechanisms are correctly accounted for, there is no need to use very complex models to accurately predict strength and fatigue life of adhesive joints. Each of the underlying processes can be represented through relatively simple assumptions.

Acknowledgements

The authors would like to acknowledge the financial support of the Technology Strategy Board (TSB) and to thank all the partners of the BMAX project (Aviation Enterprises, Element Materials Technology, Wessex Resins & Adhesives and CYTEC) for the fruitful conversations and technical support. Financial support to Jonathan Belnoue via the EPSRC Institutional Sponsorship 2012 Award (Grant number: EP/K503484/1) is also greatly acknowledged. Supporting data may be requested from Prof. S.R. Hallett. Access to supporting data may be granted, subject to consent being requested and granted from the original project participants.

References

[1] Davis M, Bond D. Principles and practices of adhesive bonded structural joints and repairs. Int J Adhes Adhes 1999;19:91–105.
[2] Adams RD. Adhesive bonding: science, technology and applications. Bristol: Woodhead Publishing Ltd; 2005.
[3] Khoramishad H, Crocombe AD, Katnam KB, Ashcroft IA. A generalised damage model for constant amplitude fatigue loading of adhesively bonded joints. Int J Adhes Adhes 2010;30:513–21.
[4] Katnam KB, Crocombe AD, Khoramishad H, Ashcroft IA. Load ratio effect on the fatigue behaviour of adhesively bonded joints: an enhanced damage model. J Adhes 2010;86:257–72.
[5] Khoramishad H, Crocombe AD, Katnam KB, Ashcroft IA. Predicting fatigue damage in adhesively bonded joints using a cohesive zone model. Int J Fatigue 2010;32:1146–58.
[6] de Moura MFSF, Gonçalves JPM. Cohesive zone model for high-cycle fatigue of adhesively bonded joints under mode I loading. Int J Solids Struct 2014;51:1123–31.
[7] de Moura MFSF, Gonçalves JPM. Development of a cohesive zone model for fatigue/fracture characterization of composite bonded joints under mode II loading. Int J Adhes Adhes 2014;54:224–30.
[8] Pirondi A, Giuliese G, Moroni F, Bernasconi A, Jamil A. Comparative study of cohesive zone and virtual crack closure techniques for three-dimensional fatigue debonding. J Adhes 2014;90:457–81.
[9] Pirondi A, Giuliese G, Moroni F. Development of a cohesive zone model for three-dimensional simulation of joint de-bonding/delamination under mixed-mode I/II fatigue loading. Int J Struct Integr 2014;5:171–86.
[10] Moroni F, Pirondi A. A procedure for the simulation of fatigue crack growth in adhesively bonded joints based on a cohesive zone model and various mixed-mode propagation criteria. Eng Fract Mech 2012;89:129–38.
[11] Belnoue JP-H, Hallett SR. Cohesive/adhesive failure interaction in ductile adhesive joints Part I: A smeared-crack model for cohesive failure. Int J Adhes Adhes 2016, in press.
[12] Hart-Smith LJ, The design of repairable advanced composite structures, Proceedings of the SAE aerospace technical conference, Long Beach, CA, USA; 1985.
[13] Pardoen T, Ferracin T, Landis CM, Delannay F. Constraint effects in adhesive joint fracture. J Mech Phys Solids 2005;53:1951–83.

[14] Martiny P, Lani F, Kinloch AJ, Pardoen T. A multiscale parametric study of mode I fracture in metal-to-metal low-toughness adhesive joints. Int J Fract 2012;173:105–33.
[15] Martiny P, Lani F, Kinloch AJ, Pardoen T. Numerical analysis of the energy contributions in peel tests: a steady-state multilevel finite element approach. Int J Adhes Adhes 2008;28:222–36.
[16] Jiang W-G, Hallett SR, Green BG, Wisnom MR. A concise interface constitutive law for analysis of delamination and splitting in composite materials and its application to scaled notched tensile specimens. Int J Numer Methods Eng 2007;69:1982–95.
[17] Harper PW, Hallett SR. A fatigue degradation law for cohesive interface elements – development and application to composite materials. Int J Fatigue 2010;32:1774–87.
[18] Gan KW, Hallett SR, Wisnom MR. Measurement and modelling of interlaminar shear strength enhancement under moderate through-thickness compression. Compos Part A: Appl Sci Manuf 2013;49:18–25.
[19] Cognard JY, Créac'hcadec R, Maurice J, Davies P, Peleau M, da Silva LFM. Analysis of the influence of hydrostatic stress on the behaviour of an adhesive in a bonded assembly. J Adhes Sci Technol 2010;24:1977–94.
[20] Kawashita LF, Hallett SR. A crack tip tracking algorithm for cohesive interface element analysis of fatigue delamination propagation in composite materials. Int J Solids Struct 2012;49:2898–913.
[21] Turon A, Costa J, Camanho PP, Dávila CG. Simulation of delamination in composites under high-cycle fatigue. Compos Part A: Appl Sci Manuf 2007;38:2270–82.
[22] Muñoz JJ, Galvanetto U, Robinson P. On the numerical simulation of fatigue driven delamination with interface elements. Int J Fatigue 2006;28:1136–46.
[23] Roe KL, Siegmund T. An irreversible cohesive zone model for interface fatigue crack growth simulation. Eng Fract Mech 2003;70:209–32.
[24] Russell AJ, Street KN. Predicting interlaminar fatigue crack growth rates in compressively loaded laminates. In: Composite materials: fatigue and fracture, second volume, 1012. Philadelphia: American Society for Testing and Materials; 1989. p. 162–78.
[25] Blanco N, Gamstedt EK, Asp LE, Costa J. Mixed-mode delamination growth in carbon–fibre composite laminates under cyclic loading. Int J Solids Struct 2004;41:4219–35.
[26] Giannis S. Utilising fracture mechanics principles for predicting the mixed-mode delamination onset and growth in tapered composite laminates. Compos Struct 2013;102:294–305.
[27] Van Der Meer FP, Sluys LJ, The influence of friction and plasticity on mode II delamination fracture toughness, Proceedings of CFRAC 2013. Prague, Czech Republic: The Czech Technical University in Prague, Faculty of Civil Engineering; 2013. p. 143.
[28] Pascoe JA, Alderliesten RC, Benedictus R. Methods for the prediction of fatigue delamination growth in composites and adhesive bonds – a critical review. Eng Fract Mech 2013;112–113:72–96.